An experimental study of hydroxylbastnasite solubility in aqueous solutions at 25 °C

Martin Voigt [a,*], Juan Diego Rodriguez-Blanco [b], Beatriz Vallina [c], Liane G. Benning [c,d], Eric H. Oelkers [a,e]

[a] GET/CNRS, 14 avenue Édouard Belin, 31400 Toulouse, France
[b] Nano-Science Center, University of Copenhagen, Universitetsparken 5, 2100 København, Denmark
[c] School of Earth and Environment, University of Leeds, Leeds LS2 9JT, United Kingdom
[d] GFZ - Helmholz Centre Potsdam, Telegrafenberg, 14473 Potsdam, Germany
[e] Earth Sciences, UCL, Gower Street, London, United Kingdom

ARTICLE INFO

ABSTRACT

The mobility of rare earth elements (REEs) in natural aqueous solutions is of increasing interest due to their application in numerous high-tech and renewable energy technologies (e.g., wind turbines and electric vehicles), as well as their role as tracers in the Earth Sciences. Basic thermodynamic data for water–rock interactions are, however, sparse and partially inconsistent, even for carbonate minerals of the bastnasite group ($REE(CO_3)(OH,F)$), which currently represent the most exploited REE ore. Towards the improved quantification of the REE in natural and industrial systems, pure hexagonal hydroxylbastnasite and orthorhombic kozoite ($REE(CO_3)(OH)$) were synthesized at hydrothermal conditions and subsequently used as starting material for aqueous dissolution and precipitation experiments. All closed system experiments were performed in air equilibrated aqueous fluids. Reaction progress was followed by measuring pH and REE concentrations at regular intervals. Experiments at 25 °C in the presence of selected concentrations of HCl and NaOH were run for up to 33 days until steady-state pH and REE concentrations were attained. Results indicate that the solubility products (K_{SP}) of the reaction $REE(CO_3)(OH) = REE^{3+} + CO_3^{2-} + OH^-$ are $\log(K_{SP}) = -23.8 \pm 0.1$, -24.1 ± 0.3, and -22.3 ± 0.2 for Nd-, La-hydroxylbastnasite, and Nd-kozoite, respectively at 25 °C.

© 2016 Elsevier B.V. All rights reserved.

1. Introduction

The rare earth elements (REEs) are of particular interest due to their various applications in geosciences and high-technology components (e.g., Binnemans et al., 2013; Jordens et al., 2013; McLellan et al., 2013; Preinfalk and Morteani, 1989). Their use as tracers of geological processes arises from their relatively similar chemical behaviour but gradually decreasing ionic size from lanthanum to lutetium, leading to distinct REE concentration patterns of the REE in the different phases (e.g., Elderfield et al., 1990; Lipin and McKay, 1989; Schnetzler and Philpotts, 1970). If these signatures are preserved, they can help identify the provenance and nature of processes that lead to their formation (e.g., Elderfield and Greaves, 1982; Mckenzie and Onions, 1991; Taylor and Mclennan, 1995). Furthermore, the study of REE bearing minerals can help identify metamorphic or metasomatic processes in a variety of natural settings (e.g., Gysi et al., 2015; Harlov et al., 2010). Apart from scientific applications, there is an increasing demand for REEs as they can be exploited to create high strength permanent magnets, phosphors for electronic displays and various components in renewable energy technologies (Jordens et al., 2013). Along with monazite, xenotime,

and ion-adsorbed clays, the mineral bastnasite ($REE(F,OH)CO_3$) is one of the main ores exploited for the rare earths, with the majority currently mined in China (Jordens et al., 2013; Wang et al., 2015; Wübbeke, 2013). Major deposits of this carbonate mineral are found in association with carbonatites, peralkaline granites and syenites, veins/breccia, or, as in the case of the largest REE mine Bayan Obo (China), in sedimentary formations that underwent periods of magmatic, metamorphic and metasomatic overprint (Migdisov and Williams-Jones, 2014; Smith et al., 2015; Williams-Jones and Wood, 1992). Naturally occurring bastnasite is usually close in composition to its fluoro endmember ($REEFCO_3$) with lower low amounts of OH^- present, causing interest in fluoride-bearing aqueous solutions (Migdisov et al., 2009). Apart from this economic interest, the hydroxylbastnasite endmember ($REEOHCO_3$), as well as other rare earth element hydroxides and carbonates, are of interest due to their potential for nuclear waste storage (Rorif et al., 2005); the rare earths can be used as an analogue for long-lived actinides due to their similar electron configuration, motivating experiments aiming at predicting their behaviour (e.g., Rorif et al., 2005; Runde et al., 1992; Stipp et al., 2006). The REEs can also form as fission products. As such, REE hydroxides or carbonates could form from the interaction of nuclear waste with natural waters, and thereby serve as potential host minerals for long-lived actinides (Rorif et al., 2005).

* Corresponding author.
  E-mail address: martin.voigt@get.obs-mip.fr (M. Voigt).

Despite its role in a plethora of processes, relatively few studies have assessed the stability of hydroxylbastnasite in presence of aqueous solutions. Although several studies have measured the solubility of the orthorhombic polymorph kozoite (REEOHCO$_3$; Carroll, 1993; Meinrath and Kim, 1991; Meinrath and Takeishi, 1993; Runde et al., 1992) no study to date has directly measured hydroxylbastnasite solubility in aqueous solutions, and it is not clear which polymorph is thermodynamically stable at low temperature conditions. The thermodynamic properties of hydroxylbastnasite were inferred, however, from thermochemical data by Rorif et al. (2005). Towards the improved description of the behaviour of the rare earth elements in natural systems we have carried out a series of experiments at 25 °C to assess the solubility of the two REEOHCO$_3$ polymorphs hydroxylbastnasite and kozoite via dissolution and precipitation experiments in aqueous solutions and in presence of CO$_2$. This experimental data will enable comparison of the stability of both REEOHCO$_3$ polymorphs. The purpose of this manuscript is to report the results of these experiments and use these to assess the stability of these minerals in low-temperature natural systems.

2. Methods

2.1. Synthesis of starting materials

Pure Nd- and La-hydroxylbastnasite, and Nd-kozoite crystals were synthesized hydrothermally as described by Vallina et al. (2014) to obtain minerals with pure end-member compositions. Briefly, aqueous solutions with a concentration of 50 mM of the desired REE-chloride were mixed with 50 mM Na$_2$CO$_3$ solutions at ambient temperature, provoking the immediate precipitation of an amorphous rare earth element carbonate phase. This material was subsequently heated to 165 °C in titanium reactors placed in rocking furnaces or in Teflon-lined reactors that were manually shaken at regular intervals. This procedure was performed at saturated water-vapour pressure using slow heating rates where the final temperature was reached in approximately 100 min. Synthesis was carried out at 165 °C to promote the formation of micrometric-sized crystals, because at higher temperatures the formation of spherulites (consisting of nanometric sized crystals) is promoted (Vallina et al., 2015). At 165 °C hydroxylbastnasite forms from kozoite by dissolution–recrystallisation, a relatively slow growth process (hours–days) compared to spherulitic growth (seconds–minutes). Synthesis products were quenched after 1 to 4 weeks, filtered through 0.22 μm membrane filters, washed with ultrapure water and isopropanol and dried at ambient temperature. Synthesis of both hydroxylbastnasite and kozoite, was possible by seeding the solutions with previously produced crystals of the selected mineral. The synthesis of hydroxylbastnasite and kozoite end-members with heavier REEs was not possible using this method, presumably due to their distinct in ionic radii.

The crystalline products were analysed by X-ray diffraction (XRD) to verify the crystal structure and by scanning electron microscopy (SEM) to examine the size and shape of the individual crystals. Crystal size was >5 μm (Fig. 1), so that the influence of particle size on solubility is expected to be negligible. For all syntheses, the powder was found to be entirely composed of either hydroxylbastnasite or kozoite within the detection limit of approximately 0.1% by comparison to the structural data of Ni et al. (1993) and Tahara et al. (2007), respectively (Fig. 2).

2.2. Experimental design

All solubility experiments were performed at 25 ± 1 °C using reactors immersed in a thermostatically controlled water bath (Fig. 3). The temperature was restricted to 25 °C in this study because of the lack of precise stability constants for aqueous rare earth element complexes in aqueous solutions at higher temperatures: The interpretation of a preliminary dissolution experiment, carried out at 110 °C in a closed titanium reactor in equilibrium with a fixed CO$_2$ pressure of 500 kPa indicated that uncertainties associated with available REE complex stability constants are larger than the difference in the solubility product between 110 °C and 25 °C. The experimental aqueous solutions were kept in 1 L polyethylene (PE) reactors and mixed with fish-clip stir bars (Bürkle GmbH) to avoid the grinding of the solids. Reactive fluid equilibrium with a constant CO$_2$ partial pressure (pCO$_2$) of log(pCO$_2$) = -3.30 ± 0.04 was maintained by bubbling air into the aqueous solution using a peristaltic pump. To minimize fluid loss during the experiment, the air was pre-saturated with water vapour by bubbling it through ultrapure water (resistivity of 18.2 MΩ) twice before bubbling it into the reactor, and the gas outlet of the reactor was equipped with an air-cooled condenser (Fig. 3). All parts of the reactors and the sampling vials were cleaned prior to each experiment by soaking them in a solution comprised of 1 M HCl and ultrapure water for one day and subsequent repeated rinsing with ultrapure water. Experimental fluids were prepared with ultrapure water, bi-distilled HCl or reagent grade NaOH to attain the pH of interest, and reagent grade NaCl was added to adjust the ionic strength (I). Sampling was carried out with a polypropylene syringe and sampled fluids were immediately filtered through a 0.45 μm cellulose acetate membrane.

For dissolution experiments, the reactive fluids were sampled after approximately 1 week before the addition of the mineral powder to monitor experimental blank concentrations. Next, 0.15 g or 0.05 g of the desired mineral powder was added to the reactor for experiments at pH below and above 7, respectively. Sampling of approximately 5 mL of the fluid phase was carried out at regular intervals to monitor the temporal evolution of pH and REE concentrations. Experiments were terminated after steady state was achieved, indicated by both parameters showing no significant change over a time period of at least 4 days. For some experiments, HCl was added subsequently to the fluid phase to decrease pH and to achieve a new steady state at another
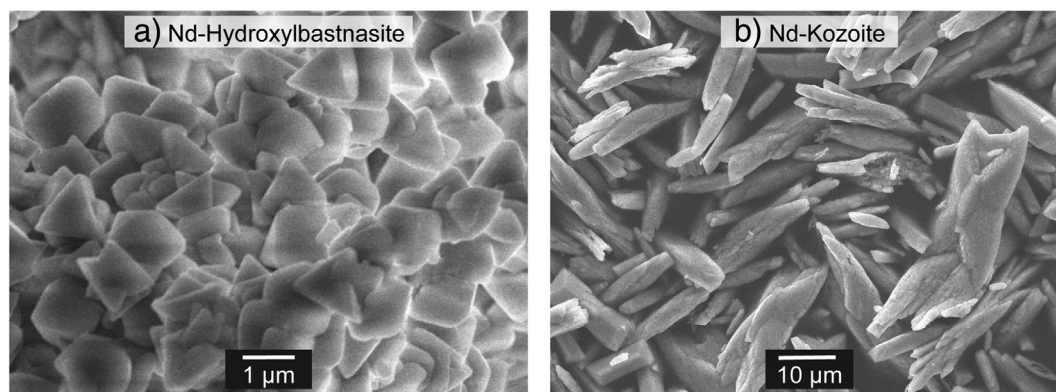

Fig. 1. SEM images of hydrothermally synthesized (a) Nd-hydroxylbastnasite and (b) Nd-kozoite. The pictures were taken in secondary electron imaging mode.
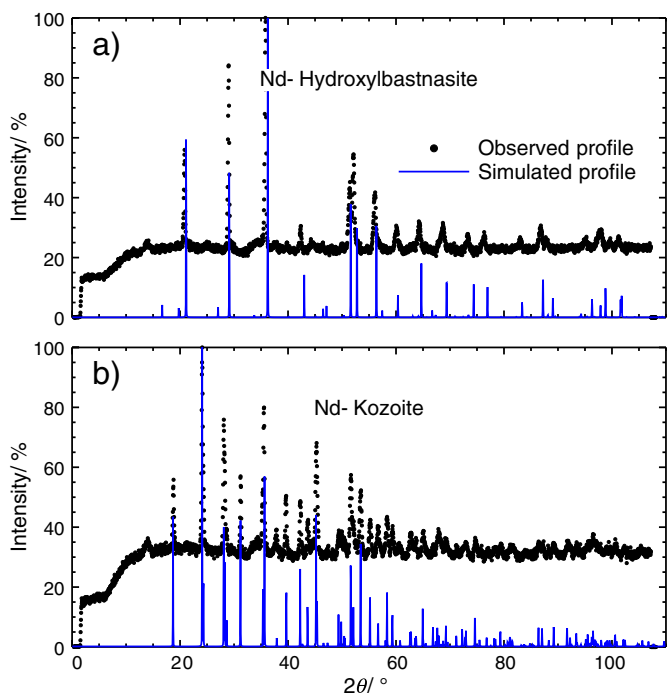
Fig. 2. XRD spectra (relative intensities vs. 2Θ, Co-Kα) of hydrothermally synthesized (a) Nd-hydroxylbastnasite and (b) Nd-kozoite (symbols) compared to synthetic XRD patterns calculated from the structural data of Ni et al. (1993) and Tahara et al. (2007) (blue lines). (For interpretation of the references to color in this figure legend, the reader is referred to the web version of this article.)

pH. Due to sampling, the volumes of the reactive fluids decreased from an initial 385 ± 30 mL, but always remained more than 75% of this initial value. After each experiment, the remaining powder was filtered, rinsed with ultrapure water multiple times, dried at ambient temperature, and examined by XRD and SEM to verify that no phase change occurred during the experiment.

To verify thermodynamic equilibrium, precipitation experiments were carried out as well. For these experiments, the reactive fluid pH

of a dissolution experiment that already attained steady state was increased by adding a small volume of NaOH to the fluid phase. This induced the precipitation of a REE carbonate phase due to its decreasing solubility with increasing pH. Fluid sampling was performed to monitor attainment of a new steady state by applying the same criteria as in dissolution experiments. At the end of these experiments, the solids were filtered and dried, and analysed by XRD.

2.3. Analytical methods

The pH of all sampled fluids was measured in situ using a VWR double junction epoxy electrode. For each pH measurement, the solution was stirred until a stable potential was attained. Subsequently, stirring was stopped and the potential was recorded when it restabilized (generally this required less than 10 s). Stirring was stopped to avoid the build-up of stirring potentials in the low ionic-strength solutions; this method was found to yield reproducible results. The pH electrode was calibrated with three NIST traceable pH buffer solutions (pH 4.0, 6.9, 9.2, Fluka) before each use at the experimental temperature. Different ionic strengths of the pH buffers and experimental solutions can potentially lead to a measurement bias due to the different liquid junction potentials. However, no correction for this bias was applied, because its magnitude is likely smaller than the uncertainty of the pH measurements (Kadis and Leito, 2010).

Aqueous rare earth element concentrations were determined by Inductively Coupled Plasma-Mass Spectrometry (ICP-MS) using a Thermo Scientific Element XR or Agilent 7500ce. Prior to analysis, samples were acidified to ~0.37 mol/kg HNO_3 using bi-distilled acid, and known concentrations of In and Re were added as internal standards. Standards were prepared using NIST traceable PlasmaCal single element standards (SCP Science). Detection limits, determined by analysis of blanks that were subjected to the same experimental and analytical procedures as actual samples, are approximately 2×10^{-11} mol/kg. Gaseous CO_2 concentrations were determined with a non-dispersive infra-red (NDIR) CO_2 gas analyser (model LI-820, LICOR Inc.). Solid experimental products were analysed by X-ray powder diffraction using a Co source and by SEM using a Quanta 3D FEG or Jeol JSM 6360LV equipped with an energy-dispersive X-ray spectrometer (EDS).
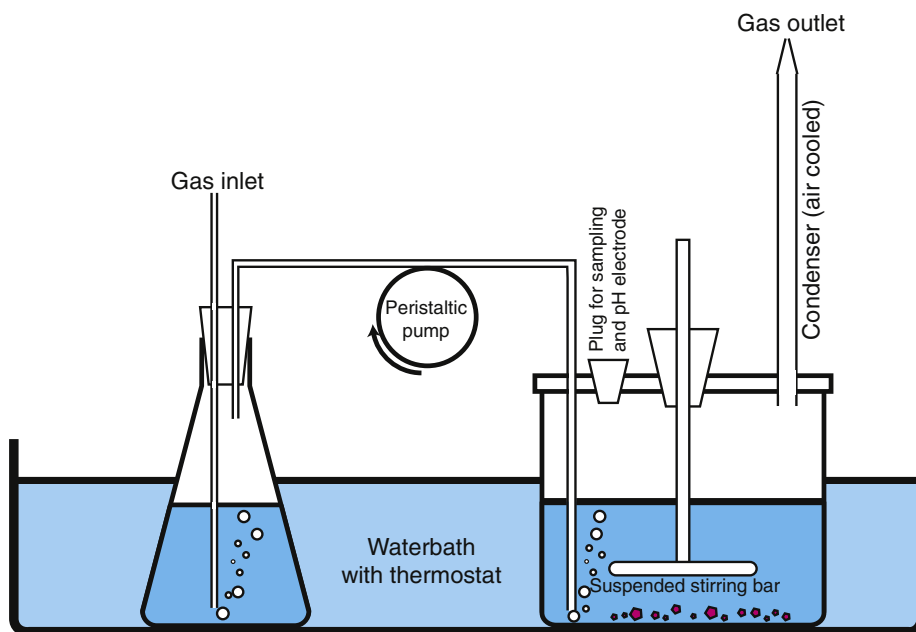

Fig. 3. Schematic image of the experimental reactor. The mineral was placed in a thermostatically controlled reactor together with the aqueous solution, which was agitated using a suspended stirring bar. Equilibrium with a constant CO_2 partial pressure was achieved by bubbling presaturated air into the reactor with a peristaltic pump. Evaporation was minimized by an air-cooled condenser.

2.4. Thermodynamic modelling

Thermodynamic calculations of systems at equilibrium were performed using the PHREEQC software package (Parkhurst and Appelo, 2013) together with its Lawrence Livermore National Laboratory (LLNL) database (Johnson et al., 2000). Standard state for solid phases and H_2O is the pure phase, while a hypothetical 1 m aqueous solution referenced to infinite dilution is chosen for unit activity of aqueous species, both at the temperature and pressure of interest. The Livermore National Laboratory aqueous model (Daveler and Wolery, 1992), which uses the extended Debye-Hückel equation of Helgeson (1969) was used to calculate activity coefficients. Due to the low ionic strengths of all experimental fluids considered in this study, the choice of activity model does not significantly affect retrieved reaction quotients. We chose the Helgeson (1969) activity model to insure all calculations were consistent with the LLNL database. Since the only aqueous REE complexes present in significant amounts in the experimental solutions are $REECO_3^+$ and $REE(CO_3)_2^-$, the total (measured) REE concentration can be expressed as $c_{REE} = c_{REE^{3+}} + c_{REECO_3^+} + c_{REE(CO_3)_2^-}$. This allows the calculation of $c_{REE^{3+}}$, the activity $a_{REE^{3+}}$ and thus the solubility products of the minerals of interest using the stability constants of the complexes and the activity model. The stability constants for the $REECO_3^+$ and $REE(CO_3)_2^-$ aqueous complexes were taken from Ohta and Kawabe (2000) and listed in Table 1 with other equilibrium constants used in this study. To assess the uncertainty of PHREEQC calculations caused by uncertainty in input parameters, Monte Carlo type simulations were run using the IPhreeqc modules (Charlton and Parkhurst, 2011) in combination with Wolfram Mathematica.

3. Results

3.1. Evolution of aqueous solution compositions and solids

Experimental parameters as well as reactive aqueous solution compositions at steady state are listed in Table 2. During the dissolution experiments, stable pH and aqueous REE concentrations were attained after 6 to 33 days (Fig. 4). A decrease of dissolution rates with increasing pH was observed, however the lack of information on the specific surface areas of the reacting solids, as well as large sampling intervals in some experiments prevent the quantification of mineral dissolution rates from these data. The appearance of the minerals used in dissolution experiments remained unchanged under the SEM, and XRD patterns were identical before and after the experiments.

In experiments where the precipitation of hydroxylbastnasite or kozoite was induced, the addition of NaOH caused a rapid decrease of

Table 1
Values of equilibrium constants of reactions used in the thermodynamic calculations, as well as the solubility products obtained in this study (cf. Section 3.3 'Solubility product calculations'). HB: Hydroxylbastnasite.

Reaction	log K	Source
$La^{3+} + CO_3^{2-} = LaCO_3^+$	12.52	Ohta and Kawabe (2000)
$La^{3+} + 2CO_3^{2-} = La(CO_3)_2^-$	8.33	Ohta and Kawabe (2000)
$Nd^{3+} + CO_3^{2-} = NdCO_3^+$	13.59	Ohta and Kawabe (2000)
$Nd^{3+} + 2CO_3^{2-} = Nd(CO_3)_2^-$	8.75	Ohta and Kawabe (2000)
$CO_{2(g)} + H_2O = H^+ + HCO_3^-$	−7.8136	Johnson et al. (2000)
$HCO_3^- + H^+ = CO_{2(aq)} + H_2O$	6.3447	Johnson et al. (2000)
$HCO_3^- = H^+ + CO_3^{2-}$	−10.3288	Johnson et al. (2000)
$H_2O = H^+ + OH^-$	−13.9951	Johnson et al. (2000)
$NdOHCO_{3(HB)} \rightarrow REE^{3+} + OH^- + CO_3^{2-}$	−23.8 ± 0.1	This study
$LaOHCO_{3(HB)} \rightarrow REE^{3+} + OH^- + CO_3^{2-}$	−24.1 ± 0.3	This study
$NdOHCO_{3(Kozoite)} \rightarrow REE^{3+} + OH^- + CO_3^{2-}$	−22.3 ± 0.2	This study

aqueous REE concentrations followed by the stabilization of pH and REE concentrations (Fig. 5). Analysis of the precipitated solids by XRD showed that kozoite precipitated from aqueous solutions having a pH below 7, even if hydroxylbastnasite was present in the reactor from the dissolution stage of the experiment. However, it was possible to precipitate hydroxylbastnasite at higher pH, as confirmed by the presence of only hydroxylbastnasite by XRD in the solid materials recovered from these experiments.

3.2. Stoichiometry of dissolution

Since both hydroxylbastnasite and kozoite release hydroxyl ions during dissolution, the reactive fluid pH can be used to assess the stoichiometry of dissolution. This can be illustrated by calculating the pH of the experiments based on thermodynamic considerations (see Section 2.4 'Thermodynamic modelling' for details) using the measured aqueous REE concentrations and initial reactive aqueous solution composition and assuming stoichiometric dissolution. The comparison of these calculated pH, which assume stoichiometric dissolution, with measured pH is shown in Fig. 6. These results demonstrate that there is no systematic preferential release of REE ions compared to OH^- from the minerals, consistent with stoichiometric dissolution. It can also be seen that the uncertainty of the calculated pH is higher at lower pH. This is caused by the increasing dependence of the pH on the mass of $REEOHCO_3$ dissolved (calculated using measured REE concentrations, which are subject to analytical uncertainties) with decreasing pH because of the lower absolute amount of OH^- in the aqueous solution.

3.3. Solubility product calculations

Our experimental data of aqueous solutions in equilibrium with hydroxylbastnasite and kozoite (Table 2) allow the calculation of the solubility products (K_{SP}) of these minerals at 25 °C, defined by

$$K_{SP} = a_{REE^{3+}} \cdot a_{OH^-} \cdot a_{CO_3^{2-}}$$

where a_i are the activities of the aqueous species i, corresponding to the dissolution reaction

$$REEOHCO_{3(s)} \rightarrow REE^{3+} + OH^- + CO_3^{2-}.$$

Calculation of activities were carried out in PHREEQC (see Section 2.4 'Thermodynamic modelling' for details), and the resulting K_{SP} of the individual experiments are listed in Table 2. The logarithms of the mean solubility products are −23.8 ± 0.1, −24.1 ± 0.3, and −22.3 ± 0.2 for Nd-hydroxylbastnasite, La-hydroxylbastnasite, and Nd-kozoite, respectively (cf. Table 1). The values for hydroxylbastnasite are in close agreement with corresponding solubility products calculated from calorimetric data by Rorif et al. (2005), which are −23.7 ± 0.6, −23.3 ± 0.6 for the Nd and La endmembers, respectively. The solubility product of Nd-kozoite, which was previously determined by Carroll (1993) as −21.7 ± 0.3 (converted from the originally published dissolution reaction version using thermodynamic data described in Section 2.4 'Thermodynamic modelling') is also close to that determined from our experiments. Runde et al. (1992) determined a value of $log(K_{SP}) = -19.94 ± 0.16$ for orthorhombic $NdOHCO_3$ in 0.1 M ionic strength aqueous solution, which was converted to zero ionic strength by Rorif et al. (2005), yielding a value of −21.4 ± 0.3. Similarly, Rorif et al. (2005) report $log(K_{SP})$ at zero ionic strength of −20.7 ± 0.2 and −21.6 ± 0.4, calculated from data reported by Meinrath and Kim (1991) and Meinrath and Takeishi (1993), respectively. These three values are slightly higher than that determined in this study. This difference might be caused by the lack of reversal of thermodynamic equilibrium in these past studies, which approached the solubility only from supersaturation.

Table 2

Characteristics of dissolution and precipitation experiments performed in aqueous solutions at 25 °C and in equilibrium with atmospheric CO_2 $\log(pCO_2) = -3.30 \pm 0.04$. pH and REE concentrations are the final values measured after attainment of steady state, and $\log(K_{SP})$ values were calculated using the procedure explained in the text. Reported uncertainties are one standard deviation, which were calculated from uncertainties in measured parameters using a Monte Carlo method in the case of $\log(K_{SP})$. The term Nd/La-HB refers to Nd/La-Hydroxylbastnasite. Experiments that begin with the same prefix (e.g. C013B-05 and C013B-19) represent individual samples collected from the same reactor, for which a new equilibrium was established by addition of small amounts of HCl or NaOH and subsequent dissolution or precipitation of the mineral of interest (see Section 2.2 'Thermodynamic modelling').

Exp. number	Mineral	pH (final)	REE/(mol/kg)	NaCl/(mol/kg)[a]	HCl/(mol/kg)[a]	NaOH/(mol/kg)[a]	I/(mol/L)	$\log(K_{SP})$
Dissolution experiments								
C012A	Nd-HB	5.07 ± 0.04	$(3.3 \pm 0.2) \times 10^{-4}$	0	$(1.08 \pm 0.07) \times 10^{-3}$	0	$(2.1 \pm 0.1) \times 10^{-3}$	-24.0 ± 0.2
C013A-05	Nd-HB	6.03 ± 0.09	$(3.8 \pm 0.4) \times 10^{-6}$	$(9.67 \pm 0.03) \times 10^{-4}$	0	0	$(9.87 \pm 0.04) \times 10^{-4}$	-23.1 ± 0.3
C013B-05	Nd-HB	5.91 ± 0.09	$(2.3 \pm 0.1) \times 10^{-6}$	$(9.70 \pm 0.03) \times 10^{-4}$	0	0	$(9.83 \pm 0.03) \times 10^{-4}$	-23.6 ± 0.3
C013A-11	Nd-HB	5.31 ± 0.09	$(3.6 \pm 0.2) \times 10^{-5}$	$(9.67 \pm 0.03) \times 10^{-4}$	$(1.005 \pm 0.006) \times 10^{-4}$	0	$(1.174 \pm 0.005) \times 10^{-3}$	-24.2 ± 0.3
C015	Nd-HB	7.16 ± 0.09	$(6.5 \pm 0.3) \times 10^{-9}$	$(1.001 \pm 0.004) \times 10^{-3}$	0	$(9.7 \pm 0.2) \times 10^{-5}$	$(1.098 \pm 0.004) \times 10^{-3}$	-23.86 ± 0.03
C029	Nd-HB	8.10 ± 0.04	$(1.38 \pm 0.05) \times 10^{-9}$	$(1.0 \pm 0.2) \times 10^{-3}$	0	$(1.05 \pm 0.01) \times 10^{-3}$	$(2.1 \pm 0.2) \times 10^{-3}$	-23.65 ± 0.02
C021-05	La-HB	5.78 ± 0.04	$(5.29 \pm 0.06) \times 10^{-6}$	$(1.00 \pm 0.02) \times 10^{-2}$	0	0	$(1.00 \pm 0.02) \times 10^{-2}$	-23.8 ± 0.1
C021-15	La-HB	5.29 ± 0.04	$(3.98 \pm 0.04) \times 10^{-5}$	$(1.00 \pm 0.02) \times 10^{-2}$	$(1.02 \pm 0.02) \times 10^{-4}$	0	$(1.02 \pm 0.03) \times 10^{-2}$	-24.4 ± 0.1
C022	Nd-Kozoite	5.70 ± 0.04	$(3.17 \pm 0.07) \times 10^{-4}$	$(8.9 \pm 0.2) \times 10^{-3}$	$(1.01 \pm 0.01) \times 10^{-3}$	0	$(1.09 \pm 0.02) \times 10^{-2}$	-22.3 ± 0.1
Precipitation experiments								
C013B-11	Nd-HB	7.10 ± 0.09	$(3.5 \pm 0.2) \times 10^{-9}$	$(9.70 \pm 0.03) \times 10^{-4}$	0	$(10.0 \pm 0.2) \times 10^{-5}$	$(1.070 \pm 0.003) \times 10^{-3}$	-24.12 ± 0.03
C013B-19	Nd-HB	8.22 ± 0.09	$(6.7 \pm 0.3) \times 10^{-10}$	$(9.70 \pm 0.03) \times 10^{-4}$	0	$(9.72 \pm 0.06) \times 10^{-4}$	$(1.945 \pm 0.007) \times 10^{-3}$	-23.98 ± 0.02
C014	Nd-Kozoite	5.65 ± 0.05	$(4.7 \pm 0.5) \times 10^{-4}$	0	$(9.4 \pm 0.2) \times 10^{-3}$	$(7.691 \pm 0.009) \times 10^{-3}$	$(1.08 \pm 0.02) \times 10^{-2}$	-22.3 ± 0.1
C019	Nd-Kozoite	5.68 ± 0.05	$(3.95 \pm 0.03) \times 10^{-4}$	0	$(1.01 \pm 0.02) \times 10^{-2}$	$(9.0 \pm 0.1) \times 10^{-3}$	$(1.11 \pm 0.03) \times 10^{-2}$	-22.3 ± 0.2

[a] These values refer to the concentration of salts added to create the reactive fluid used in the experiment.

Fig. 7 shows modelled Nd concentrations in equilibrium with the Nd endmembers of the two minerals as function of pH, calculated using the solubility products determined in this study and assuming a $\log(pCO_2)$ of −3.30 (as in the experiments). Comparison to the experimental data shows that they are in close agreement with the predicted shape of the solubility curve. It can also be seen that dissolution and precipitation experiments are consistent with each other and with thermodynamic equilibrium.

4. Discussion

The experimental data obtained for Nd-hydroxylbastnasite and Nd-kozoite indicate that the former is more stable at 25 °C because of its lower solubility product and therefore lower chemical potential. Furthermore, no significant difference was detected between the solubilities of Nd- and La-hydroxylbastnasite. In the following two sections,

we illustrate the stability of hydroxylbastnasite in natural aqueous solutions. For this purpose, we compare the stability of hydroxylbastnasite with fluorobastnasite in presence of variable aqueous fluorine concentrations, and with monazite because of its widespread distribution in the continental crust (Poitrasson et al., 2004).

4.1. Comparison to fluorobastnasite

Bastnasite found in nature is usually compositionally closer to the fluorobastnasite endmember ($REEFCO_3$) than to hydroxylbastnasite, making a comparison of their relative solubilities especially interesting. However, a direct comparison is not possible at the moment due to the lack of direct solubility measurements of fluorobastnasite in aqueous
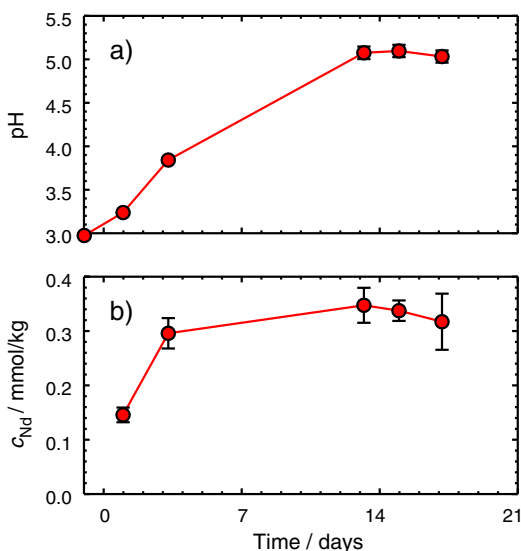
Fig. 4. Evolution of pH and aqueous Nd concentrations in dissolution experiment C012A. It can be seen that the dissolution of Nd-hydroxylbastnasite leads to an increase in Nd and pH at the beginning of the experiment, before a steady state is achieved at a later stage. Error bars show one standard deviation of the analytical data.
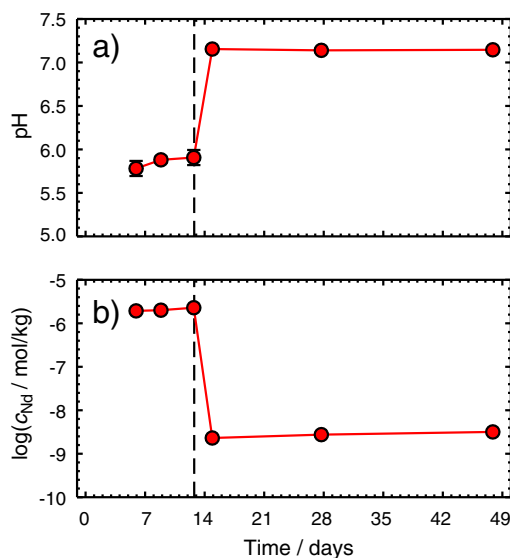
Fig. 5. Evolution of pH and aqueous Nd concentrations in precipitation experiment C013B. Nd-hydroxylbastnasite was added to the reactor in the beginning to achieve a first equilibrium at pH 5.91 ± 0.09. After approximately 13 days (dashed line), a small quantity of NaOH was added to increase the pH and a new steady state was attained, with a lower Nd concentration due to Nd-hydroxylbastnasite precipitation. Where no error bar is visible, analytical uncertainties (one standard deviation) are within the size of the symbols.
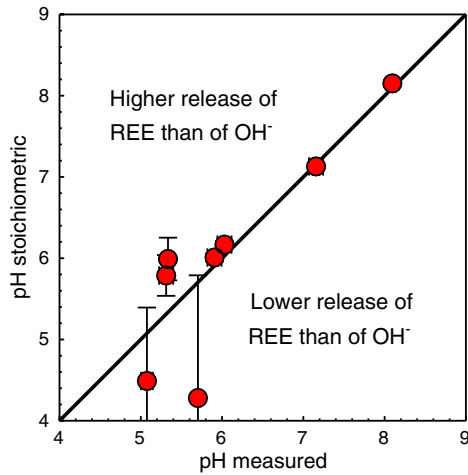
Fig. 6. Measured pH during the dissolution experiments plotted versus the pH calculated from measured REE concentrations and the initial solution composition and assuming stoichiometric dissolution. Deviations from the 1:1 line suggest an non-stoichiometric release of REE or OH⁻ from the mineral (see text). Error bars show one standard deviation, calculated with a Monte Carlo type method using analytical uncertainties.

solutions. Nonetheless, an estimate is possible using thermochemical data obtained by Gysi and Williams-Jones (2015), who used results from differential scanning calorimetric experiments on natural bastnasite (Ce$_{0.50}$La$_{0.25}$Nd$_{0.20}$Pr$_{0.05}$CO$_3$F) to calculate a Gibbs free energy of its formation at 25 °C and 1 bar of $\Delta_f G° = -1710 \pm 12$ kJ/mol for this mineral. Using the relationship

$$\ln K_{SP} = \frac{-\Delta_r G°_{diss}}{RT} = \frac{-\left(\Delta_f G°_{REE^{3+}_{(aq)}} + \Delta_f G°_{CO_3^{2-}_{(aq)}} + \Delta_f G°_{F^-_{(aq)}} - \Delta_f G°_{bastnasite} \right)}{RT}$$

where R refers to the gas constant, and adopting the Gibbs free energies of formation for the aqueous species Ce^{3+}, La^{3+}, Nd^{3+}, Pr^{3+}, F$^-$ and CO$_3^{2-}$ from Oelkers et al. (1995) as well as their estimated uncertainties of up to 600 kcal/mol in these parameters, a value of $\log(K_{SP}) = -39 \pm 2$ is obtained for fluorobastnasite of this composition. Even considering the uncertainties introduced by these calculations, and by the fact that the solubility product for fluorobastnasite was only determined

for a mixed-REE mineral, this indicates that bastnasite is stabilized considerably if fluorine is present in the aqueous solution, as demonstrated by the calculated stability fields in Fig. 8, showing that the fluorine endmember is the more stable phase even if only extremely small quantities of aqueous F⁻ are present. For the purpose of this calculation, it was assumed that the difference in solubility of the NdFCO$_3$ endmember compared to the one determined for the mixed-REE mineral by (Gysi et al., 2015) is negligible compared to the uncertainties introduced by the Gibbs free energies of formation for the aqueous species. This result is in agreement with the prevalence of fluorine-rich bastnasite in nature; hydroxylbastnasite, only forms in fluorine-poor systems (Hsu, 1992; Williams-Jones and Wood, 1992).

4.2. Comparison to monazite

Monazite (REEPO$_4$) is another common rare earth element mineral, which is of interest because of its applications in geosciences (e.g. geochronology and geothermometry) as well as due to its use as an ore mineral (e.g., Poitrasson et al., 2004). The solubility of synthetic NdPO$_4$ has been determined as $\log(K_{SP}) = -26.02$ (interpolated for 25 °C) by Poitrasson et al. (2004), allowing a direct comparison to hydroxylbastnasite. The boundary between the stability fields of the two minerals in equilibrium with aqueous solutions of variable CO$_2$ and phosphorus contents at neutral pH is shown in Fig. 9, illustrating the potential effect of different CO$_2$ partial pressures in natural systems. It was found that phosphate-REE complexes are only present in negligible quantities under these conditions, as inferred from stability constants of from Haas et al. (1995) and Millero (1992). Although precise data of phosphorus concentrations found in nature are sparse, estimates of lake water P concentrations (Hudson et al., 2000) indicate that monazite is the more stable phase in these waters in equilibrium with atmospheric CO$_2$ levels. Similar to fluorobastnasite, it can be concluded that hydroxylbastnasite is only thermodynamically more stable in phosphorous-poor conditions or at extremely high CO$_2$ partial pressures.

5. Conclusions

Dissolution and precipitation experiments of synthetic hydroxylbastnasite and kozoite (hexagonal and orthorhombic REEOHCO$_3$, respectively) were performed in aqueous solutions at 25 °C to assess
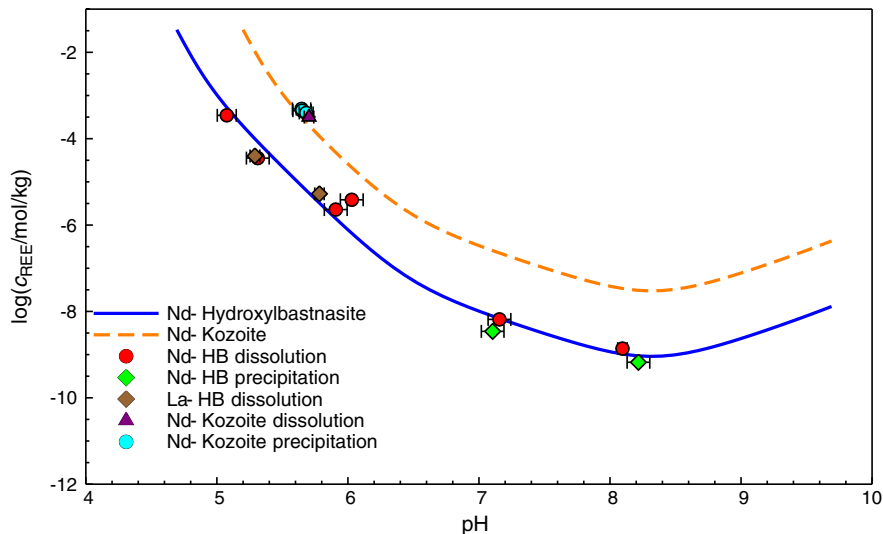

Fig. 7. Plot of aqueous REE concentrations vs. final pH of dissolution and precipitation experiments (symbols) with hydroxylbastnasite and kozoite at 25 °C in equilibrium with $\log(pCO_2) = -3.30 \pm 0.04$. The blue and orange curves show the REE concentrations in equilibrium with Nd-hydroxylbastnasite and Nd-kozoite, respectively, calculated using PHREEQC and the solubility products determined in this study. Where no error bar is visible, analytical uncertainties (one standard deviation) are within the size of the symbols. (For interpretation of the references to color in this figure legend, the reader is referred to the web version of this article.)
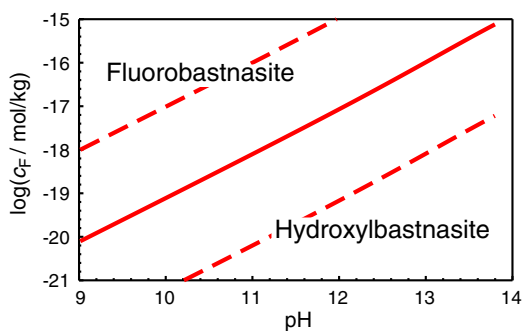
Fig. 8. Plot of the modelled aqueous F concentration in equilibrium with hydroxylbastnasite and fluorobastnasite (solid line) in aqueous solutions at 25 °C as a function of pH. The exchange reaction whose equilibrium is illustrated by the solid line can be expressed as $REEOHCO_{3(s)} + F^- \leftrightarrow REEFCO_{3(s)} + OH^-$. The dashed lines represent the uncertainties (one standard deviation), calculated from the uncertainties in the thermodynamic properties of the minerals. See text for the details of the model calculations.

the solubility of these minerals. For Nd-kozoite, the solubility product was determined to be $\log(K_{SP}) = -22.3 \pm 0.2$, which is in good agreement with data obtained previously using a similar methodology (Carroll, 1993; Meinrath and Kim, 1991; Meinrath and Takeishi, 1993; Runde et al., 1992). Our experiments showed that hydroxylbastnasite is thermodynamically stable compared to kozoite in aqueous solutions under these conditions, and the solubility product of the Nd endmember is equal to $\log(K_{SP}) = -23.8 \pm 0.1$. To our knowledge, this is the first direct determination of hydroxylbastnasite solubility in aqueous solutions, and our K_{SP} is consistent with the value calculated from calorimetric data by Rorif et al. (2005). Furthermore, it was found that the solubility of La-hydroxylbastnasite does not differ significantly from the Nd endmember within the precision achieved in this study.

Comparison of the solubility of hydroxylbastnasite with that of fluorobastnasite (inferred from calorimetric data of Gysi and Williams-Jones (2015)) shows that the fluorine endmember is stable even if only small quantities of fluorine are present in aqueous solution. This explains the prevalence of fluorine-rich bastnasite in natural environments, whereas hydroxylbastnasite only forms in fluorine-devoid systems (Hsu, 1992; Williams-Jones and Wood, 1992). Similarly, it can be seen from comparison to monazite (Poitrasson et al., 2004) hydroxylbastnasite is only stable if phosphorous concentrations are lower than commonly found in nature or if the CO_2 partial pressure is extremely high.
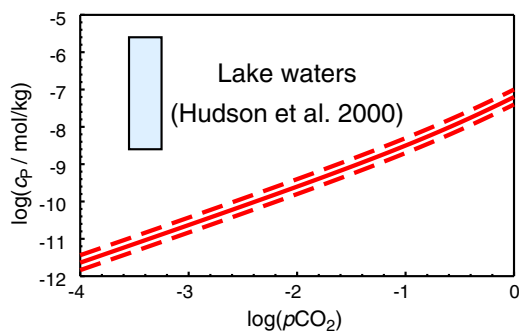

Fig. 9. Plot of the aqueous P concentrations in equilibrium with Nd-hydroxylbastnasite and Nd-monazite (solid line) in aqueous solutions at 25 °C and pH 7 as a function of pCO_2. The dashed lines represent the uncertainties (one standard deviation), calculated from the uncertainties in the thermodynamic properties of the minerals. See text for the details of the model calculations. The blue rectangle shows the approximate range of phosphorous concentrations in natural lake waters (Hudson et al., 2000) and atmospheric CO_2 concentrations. (For interpretation of the references to color in this figure legend, the reader is referred to the web version of this article.)

Although our results expand the dataset of thermodynamic stabilities of rare earth element minerals in aqueous solutions at 25 °C and provide robust values for their solubility products, there is still a lack of solubility measurements of bastnasite at higher temperatures as well as equivalent data for fluorobastnasite at 25 °C. Difficulties in K_{SP} measurements at high temperature is partly due to the lack of reliable data for the stabilities of the various aqueous complexes that REEs form with carbonate and hydroxyl ions, which are relatively small at 25 °C, but could play a major role at higher temperature (Haas et al., 1995). Furthermore, there is no available data on the dissolution and precipitation kinetics of these REE-carbonate minerals in aqueous solutions. Together with the thermodynamic stabilities determined here, such kinetic data could provide valuable information to assess the conditions of formation and preservation of natural REE mineral deposits, and help to model the fate of actinides that are released from nuclear waste storage sites.

References

Binnemans, K., Jones, P.T., Blanpain, B., Van Gerven, T., Yang, Y., Walton, A., Buchert, M., 2013. Recycling of rare earths: a critical review. J. Clean. Prod. 51, 1–22. http://dx.doi.org/10.1016/j.jclepro.2012.12.037.

Carroll, S.A., 1993. Precipitation of Nd–Ca carbonate solid solution at 25 °C. Geochim. Cosmochim. Acta 57, 3383–3393. http://dx.doi.org/10.1016/0016-7037(93)90546-9.

Charlton, S.R., Parkhurst, D.L., 2011. Modules based on the geochemical model PHREEQC for use in scripting and programming languages. Comput. Geosci. 37, 1653–1663. http://dx.doi.org/10.1016/j.cageo.2011.02.005.

Daveler, S.A., Wolery, T.J., 1992. EQPT, a data file preprocessor for the EQ3/6 software package: user's guide and related documentation (version 7.0). Lawrence Livermore Natl. Lab. UCRl-MA-110662. PT II, pp. 1–89.

Elderfield, H., Greaves, M.J., 1982. The rare earth elements in seawater. Nature 296, 214–219. http://dx.doi.org/10.1038/296214a0.

Elderfield, H., Upstill-Goddard, R., Sholkovitz, E.R., 1990. The rare earth elements in rivers, estuaries, and coastal seas and their significance to the composition of ocean waters. Geochim. Cosmochim. Acta 54, 971–991. http://dx.doi.org/10.1016/0016-7037(90)90432-K.

Gysi, A.P., Williams-Jones, A.E., 2015. The thermodynamic properties of bastnäsite-(Ce) and parisite-(Ce). Chem. Geol. 392, 87–101. http://dx.doi.org/10.1016/j.chemgeo.2014.11.001.

Gysi, A.P., Williams-Jones, A.E., Harlov, D., 2015. The solubility of xenotime-(Y) and other HREE phosphates ($DyPO_4$, $ErPO_4$ and $YbPO_4$) in aqueous solutions from 100 to 250 °C and psat. Chem. Geol. 401, 83–95. http://dx.doi.org/10.1016/j.chemgeo.2015.02.023.

Haas, J.R., Shock, E.L., Sassani, D.C., 1995. Rare earth elements in hydrothermal systems: estimates of standard partial molal thermodynamic properties of aqueous complexes of the rare earth elements at high pressures and temperatures. Geochim. Cosmochim. Acta 59, 4329–4350. http://dx.doi.org/10.1016/0016-7037(95)00314-P.

Harlov, D.E., Wirth, R., Hetherington, C.J., 2010. Fluid-mediated partial alteration in monazite: the role of coupled dissolution–reprecipitation in element redistribution and mass transfer. Contrib. Mineral. Petrol. 162, 329–348. http://dx.doi.org/10.1007/s00410-010-0599-7.

Helgeson, H.C., 1969. Thermodynamics of hydrothermal systems at elevated temperatures and pressures. Am. J. Sci. 267, 729–804. http://dx.doi.org/10.2475/ajs.267.7.729.

Hsu, D.L.C., 1992. Synthesis and stability of bastnaesites in a part of the system (Ce,La)–F–H–C–O. Mineral. Petrol. 47, 87–101. http://dx.doi.org/10.1007/BF01165299.

Hudson, J.J., Taylor, W.D., Schindler, D.W., 2000. Phosphate concentrations in lakes. Nature 406, 54–56. http://dx.doi.org/10.1038/35017531.

Johnson, J., Anderson, G., Parkhurst, D., 2000. Database "thermo.com.V8.R6.230.". Lawrence Livermore Natational Laboratory, Livermore, California, USA.

Jordens, A., Cheng, Y.P., Waters, K.E., 2013. A review of the beneficiation of rare earth element bearing minerals. Miner. Eng. 41, 97–114. http://dx.doi.org/10.1016/j.mineng.2012.10.017.

Kadis, R., Leito, I., 2010. Evaluation of the residual liquid junction potential contribution to the uncertainty in pH measurement: a case study on low ionic strength natural waters. Anal. Chim. Acta 664, 129–135. http://dx.doi.org/10.1016/j.aca.2010.02.007.

Lipin, B.R., McKay, G.A., 1989. Geochemistry and mineralogy of rare earth elements. Rev. Mineral. Geochem. 21, 348.

Mckenzie, D., Onions, R., 1991. Partial melt distributions from inversion of rare-earth element concentrations. J. Petrol. 32, 1021–1091. http://dx.doi.org/10.1093/petrology/32.5.1021.

McLellan, B.C., Corder, G.D., Ali, S.H., 2013. Sustainability of rare earths—an overview of the state of knowledge. Minerals 3, 304–317. http://dx.doi.org/10.3390/min3030304.

Meinrath, G., Kim, J.I., 1991. Solubility products of different Am(III) and Nd(III) carbonates. Eur. J. Solid State Inorg. Chem. 28, 383–388.

Meinrath, G., Takeishi, H., 1993. Solid–liquid equilibria of Nd^{3+} in carbonate solutions. J. Alloys Compd. 194, 93–99. http://dx.doi.org/10.1016/0925-8388(93)90651-3.

Migdisov, A.A., Williams-Jones, A.E., 2014. Hydrothermal transport and deposition of the rare earth elements by fluorine-bearing aqueous liquids. Mineral. Deposita 49, 987–997. http://dx.doi.org/10.1007/s00126-014-0554-z.

Migdisov, A.A., Williams-Jones, A.E., Wagner, T., 2009. An experimental study of the solubility and speciation of the rare earth elements (III) in fluoride- and chloride-bearing aqueous solutions at temperatures up to 300 °C. Geochim. Cosmochim. Acta 73, 7087–7109.

Millero, F.J., 1992. Stability constants for the formation of rare earth-inorganic complexes as a function of ionic strength. Geochim. Cosmochim. Acta 56, 3123–3132. http://dx.doi.org/10.1016/0016-7037(92)90293-R.

Ni, Y., Hughes, J.M., Mariano, A.N., 1993. The atomic arrangement of bastnäsite-(Ce), Ce $(CO_3)F$, and structural elements of synchysite-(Ce), röntgenite-(Ce), and parisite-(Ce). Am. Mineral. 78, 415–418.

Oelkers, E.H., Helgeson, H.C., Shock, E.L., Sverjensky, D.A., Johnson, J.W., Pokrovskii, V.A., 1995. Summary of the apparent standard partial molal Gibbs free energies of formation of aqueous species, minerals, and gases at pressures 1 to 5000 bars and temperatures 25 to 1000 °C. J. Phys. Chem. Ref. Datas 24, 1401–1560. http://dx.doi.org/10.1063/1.555976.

Ohta, A., Kawabe, I., 2000. Rare earth element partitioning between Fe oxyhydroxide precipitates and aqueous NaCl solutions doped with $NaHCO_3$: determinations of rare earth element complexation constants with carbonate ions. Geochem. J. 34, 439–454. http://dx.doi.org/10.2343/geochemj.34.439.

Parkhurst, D.L., Appelo, C.A.J., 2013. Description of input and examples for PHREEQC version 3 — a computer program for speciation, batch-reaction, one-dimensional transport, and inverse geochemical calculations. U.S. Geological Survey Techniques and Methods, Book 6. U.S. Geological Survey, p. 497 (Chapter A43).

Poitrasson, F., Oelkers, E.H., Schott, J., Montel, J.-M., 2004. Experimental determination of synthetic $NdPO_4$ monazite end-member solubility in water from 21 °C to 300 °C: implications for rare earth element mobility in crustal fluids. Geochim. Cosmochim. Acta 68, 2207–2221. http://dx.doi.org/10.1016/j.gca.2003.12.010.

Preinfalk, C., Morteani, G., 1989. The industrial applications of rare earth elements. In: Möller, P.D.P., Černý, P.D.P., Saupé, P.D.F. (Eds.), Lanthanides, Tantalum and Niobium Special Publication No. 7 of the Society for Geology Applied to Mineral Deposits. Springer Berlin Heidelberg, pp. 359–370.

Rorif, F., Fuger, J., Desreux, J.F., 2005. Thermochemistry of selected trivalent lanthanide and americium compounds: orthorhombic and hexagonal hydroxycarbonates. Radiochim. Acta Int. J. Chem. Asp. Nucl. Sci. Technol. 93, 103–110. http://dx.doi.org/10.1524/ract.93.2.103.59419.

Runde, W., Meinrath, G., Kim, J.I., 1992. A study of solid–liquid phase equilibria of trivalent lanthanide and actinide ions in carbonate systems. Radiochim. Acta 58-59, 93–100. http://dx.doi.org/10.1524/ract.1992.5859.1.93.

Schnetzler, C.C., Philpotts, J.A., 1970. Partition coefficients of rare-earth elements between igneous matrix material and rock-forming mineral phenocrysts—II. Geochim. Cosmochim. Acta 34, 331–340. http://dx.doi.org/10.1016/0016-7037(70)90110-9.

Smith, M.P., Campbell, L.S., Kynicky, J., 2015. A review of the genesis of the world class Bayan Obo Fe–REE–Nb deposits, Inner Mongolia, China: multistage processes and outstanding questions. Ore Geol. Rev. 64, 459–476. http://dx.doi.org/10.1016/j.oregeorev.2014.03.007.

Stipp, S.L.S., Christensen, J.T., Lakshtanov, L.Z., Baker, J.A., Waight, T.E., 2006. Rare earth element (REE) incorporation in natural calcite: upper limits for actinide uptake in a secondary phase. Radiochim. Acta 94, 523–528. http://dx.doi.org/10.1524/ract.2006.94.9-11.523.

Tahara, T., Nakai, I., Miyawaki, R., Matsubara, S., 2007. Crystal chemistry of $RE(CO_3)OH$. Z. Krist. 222, 326–334. http://dx.doi.org/10.1524/zkri.2007.222.7.326.

Taylor, S., Mclennan, S., 1995. The geochemical evolution of the continental-crust. Rev. Geophys. 33, 241–265. http://dx.doi.org/10.1029/95RG00262.

Vallina, B., Rodriguez-Blanco, J.D., Blanco, J.A., Benning, L.G., 2014. The effect of heating rates on the morphology of crystalline neodymium carbonates. Mineral. Mag. 78, 1391–1397. http://dx.doi.org/10.1180/minmag.2014.078.6.05.

Vallina, B., Rodriguez-Blanco, J.D., Brown, A.P., Blanco, J.A., Benning, L.G., 2015. The role of amorphous precursors in the crystallization of La and Nd carbonates. Nanoscale 7, 12166–12179. http://dx.doi.org/10.1039/C5NR01497B.

Wang, X., Lei, Y., Ge, J., Wu, S., 2015. Production forecast of China's rare earths based on the generalized Weng model and policy recommendations. Resour. Policy 43, 11–18. http://dx.doi.org/10.1016/j.resourpol.2014.11.002.

Williams-Jones, A.E., Wood, S.A., 1992. A preliminary petrogenetic grid for REE fluorocarbonates and associated minerals. Geochim. Cosmochim. Acta 56, 725–738. http://dx.doi.org/10.1016/0016-7037(92)90093-X.

Wübbeke, J., 2013. Rare earth elements in China: policies and narratives of reinventing an industry. Resour. Policy 38, 384–394. http://dx.doi.org/10.1016/j.resourpol.2013.05.005.